ORIGINAL PAPER

Proton migration in portlandite inferred from activation energy of self-diffusion and potential energy curve of OH bond

Naoki Noguchi · Keiji Shinoda

Abstract A fundamental mechanism on the atomic level for self-diffusion in the proton layer of portlandite, $Ca(OH)_2$, was investigated by conducting hydrogen–deuterium (H–D) exchange diffusion experiments and by deriving potential energy curves of OH vibrations from optical absorption measurements. Synthetic single crystals of portlandite were used in H–D experiments between 250 and 450°C at 150 MPa. Arrhenius parameters for proton diffusion perpendicular to the c-axis gave a frequency factor of 1.0×10^{-10} m^2/s and activation energy of 0.61 eV (58.5 kJ/mol). The activation energy corresponds to the height of the potential barrier between two oxygen atoms across an interlayer. The potential barrier height was also theoretically estimated using the OH potential energy curve (OH-PEC) determined by optical absorption measurements. Experimental and theoretical results suggest that the potential barrier height cannot be simply determined by overlapping two OH-PECs. The potential barrier derived theoretically was 3.11 eV. This is too high for the activation energy of the proton diffusion. It implies that the interaction between a diffusing proton and the vacancy of a proton site, and the shortening of interlayer oxygen distance by thermal vibration reduce the potential barrier.

Keywords Portlandite · Self-diffusion of proton · Activation energy of diffusion · Micro Raman spectroscopy · OH potential energy curve

N. Noguchi (✉) · K. Shinoda
Department of Geosciences, Graduate School of Science,
Osaka City University, Sugimoto 3-3-138,
Sumiyoshi-ku, Osaka 558-8585, Japan
e-mail: noguchih@sci.osaka-cu.ac.jp

Introduction

Diffusion of protons in minerals often controls the macroscopic properties of minerals such as deformation, reaction kinetics, and electrical conductivity. Previous experimental studies have measured the proton diffusion coefficients of hydrous minerals by performing hydrogen–deuterium (H–D) exchange diffusion experiments on powdered samples (Ingrin and Blanchard 2006). No correlations have been reported between the proton diffusion mechanism on an atomic scale and crystal structures because diffusion coefficients along a specific crystal axis cannot be determined using powder samples. To determine the proton diffusion mechanism on an atomic scale, the diffusion coefficient along a specific crystal axis must be determined using a single crystal. In the present study, H–D exchange diffusion experiments were conducted using a single crystal of portlandite ($Ca(OH)_2$) to clarify the fundamental proton migration mechanism. Portlandite is a good model system for studying proton self-diffusion because it has a simple crystal structure.

Portlandite is isostructural with brucite, $Mg(OH)_2$ (space group: $P\overline{3}$ m1, Z = 1), which has a CdI_2 type structure. In portlandite, distorted $[CaO_6]$ octahedra are linked together by sharing edges to form a $[CaO_6]$ octahedra layer (Fig. 1a). The $[CaO_6]$ layers stack along the c-axis and a hydrogen atom bonds to each apical oxygen atom in the $[CaO_6]$ octahedra to form an OH dipole. The protons form weak hydrogen bonds with the three nearest oxygen atoms of the adjacent $[CaO_6]$ layer. Furthermore, there is a repulsive interaction between one proton and the three nearest-neighbor protons (Parise 2006). This induces disorder at the proton locations (Fig. 1b). The results of neutron diffraction experiments on portlandite (Desgranges et al. 1993; Xu et al. 2007) suggest that a proton occupies

three equivalent 6i Wyckoff sites with occupancies of 1/3. Hence, the disorder is generated by the OH dipole axis being tilted slightly relative to the c-axis. The distance between the three 6i sites is small at low pressure (0.36 Å at 150 MPa), but it increases with increasing pressure (0.94 Å at 4.5 GPa; Xu et al. 2007). Furthermore, computer simulations based on first-principle calculations (Raugei et al. 1999) have demonstrated that a proton dynamically hops between the three equivalent sites at low pressure.

The protons between two [CaO$_6$] layers form a quasi-two-dimensional hydrogen-bonding network that has a honeycomb-like structure (Fig. 1b). Proton diffusion through the honeycomb proton layer is governed by a simple diffusion process, because a proton has to overcome a single potential energy barrier to migrate to the next site in the adjacent [CaO$_6$] layer. The proton diffusion coefficient perpendicular to the c-axis indicates the macroscopic proton migration rate in a proton layer. The activation energy of diffusion in a proton layer can be determined from the diffusion coefficient. This activation energy includes the energy corresponding to the height of the single potential energy barrier because the activation energy of diffusion is generally the energy required for a diffusing atom to migrate to a neighboring site (Borg and Dienes 1988). An independent method for determining the height of the energy barrier to be cleared by diffusing atoms involves deriving it theoretically from the interatomic distance and the potential energy curve of an OH dipole (OH-PEC). In order to determine the fundamental mechanism of proton migration, the activation energy determined by H–D exchange diffusion experiments and a theoretical OH-PEC are required. The actual OH-PEC in portlandite can be estimated from optical measurements as described later.

Herein, the diffusion coefficients perpendicular to the c-axis were determined by H–D exchange diffusion experiments using a single crystal of synthetic portlandite. Its activation energy was estimated from the temperature dependence of the diffusion coefficient between 250 and 450°C under 150 MPa and the OH-PEC of portlandite was determined by optical measurements. Using the activation energy and the OH-PEC, we investigated the proton diffusion mechanism on an atomic level.

Theory of the OH-PEC

In the present study, the OH-PEC of portlandite is assumed to be described by the Morse function $U(r)$ (Morse 1929):

$$U(r) = D_e(1 - \exp[-\alpha(r - r_0)])^2, \tag{1}$$

where D_e is the dissociation energy, α is a constant, r is the O–H distance, and r_0 is the equilibrium O–H distance (=0.95 Å; Xu et al. 2007). The eigenvalue $G(n)$ of the Schrödinger equation representing the nuclei motion in OH is expressed by Eq. 2 when the Morse function is substituted for the potential term in the Schrödinger equation (Herzberg 1989):

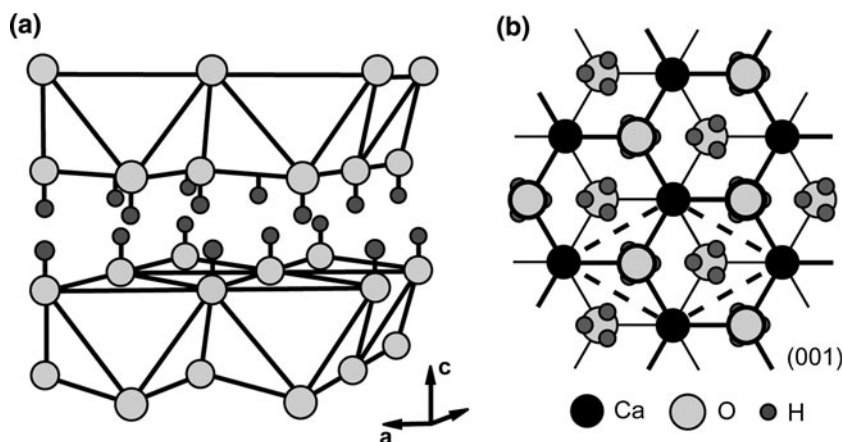$$G(n) = \left(n + \frac{1}{2}\right) h\,\omega_e - \left(n + \frac{1}{2}\right)^2 h\,\omega_e\,\chi, \tag{2}$$

where n is the vibrational quantum number, h is Plank's constant, and χ is the anharmonic coefficient. D_e and α in Eq. 1 are related to ω_e and χ by the following relations (Herzberg 1989):

$$\omega_e = \frac{\alpha}{\pi}\sqrt{\frac{D_e}{2\mu}}, \tag{3}$$

$$\chi = \frac{h\,\omega_e}{4D_e} = \frac{h\,\alpha}{4\pi\sqrt{2\,\mu\,D_e}}, \tag{4}$$

where μ is the reduced mass of the O–H bond (=1.563 × 10^{-27} kg). The OH-PEC of portlandite can be estimated from the absorption bands due to the OH

Fig. 1 Crystal structure of portlandite Ca(OH)$_2$. a Side view of the portlandite structure. A portion of two [CaO$_6$] layers and the proton layer between the [CaO$_6$] layers is shown. The protons occupy 2d Wyckoff sites. b A (001) view of a honeycomb proton layer. The *bold solid lines* and the *thin solid lines* represent the upper and lower [CaO$_6$] layers, respectively. The *broken line* indicates a unit cell. The protons occupy 6i Wyckoff sites with 1/3 occupancy

stretching vibration. Assuming that the absorption wavenumber of the nth overtone mode of the OH stretching vibration is ω_n, $G(n) - G(0)$ can be expressed as

$$G(n) - G(0) = h\,\omega_n = n\,h\,\omega_e\{1 - (1 + n)\,\chi\} \qquad (5)$$

from Eq. 2. ω_e and χ can be obtained by substituting values of ω_n into Eq. 5; the resultant D_e and α were also derived from Eqs. 3 and 4. The absorption band due to the fundamental mode (A_{2u} normal vibration) of the OH stretching vibration appears in the mid infrared (IR) region and absorption bands of overtone modes appear from the near infrared (NIR) region to the visible (VIS) region. In the present study, the OH absorption bands were measured using Fourier-transform IR (FT-IR), NIR, and VIS microspectrometers.

Experimental methods

Diffusion experiment

Single crystals of portlandite were synthesized from a supersaturated solution of $Ca(OH)_2$ in the following manner. Reagent $Ca(OH)_2$ powder (99.9%, Wako Co. Ltd.), which is slightly soluble in water at low temperature, was dissolved in ice-cold water. The solution was kept in a nitrogen evaporator at 70–80°C for 1 week, leaving single crystals of portlandite. Optically clean and hexagonal-column portlandite single crystals having a length of 50–300 μm and a diameter of 50–400 μm were synthesized. Two or three single crystals were placed in a gold capsule with 10 μL of D_2O, and the gold capsule was sealed by welding. To promote H–D exchange in portlandite, the gold capsules were placed in a cold-seal pressure vessel and annealed at 250–450°C under 150 MPa for 5–150 h (Table 1). To suppress convection in the water (the pressure medium) in the test tube and to maintain the gold capsules at a constant temperature in the vessel, a stainless-steel rod was inserted into the vessel (Boettcher and Kerrick 1971). IR absorption spectra were obtained from every fluid recovered from the gold capsule after the annealing experiments and the D_2O/H_2O ratio (c_0 in Table 1) was determined using the molar absorption coefficients of D_2O and H_2O (Venyaminov and Prendergast 1997). The D_2O/H_2O ratio is very important for accurately calculating the diffusion coefficients. The original D_2O in the gold capsule was contaminated with H_2O from the air when the gold capsule was welded.

Micro Raman spectroscopy was used to measure the deuterium diffusion profiles of the samples. Previous proton diffusion experiments used micro IR spectroscopy as the primary method for quantitatively measuring H–D diffusion profiles (Ingrin and Skogby 2000; Kurka et al. 2005). This is

Table 1 Experimental conditions and proton diffusion coefficients

Run no.	T (°C)	P (MPa)	t (h)	c_0^a	Direction	D (m²/s)
616	250	150	145	0.70	[210]	$(7.3 \pm 0.9) \times 10^{-17}$
124	250	150	91	0.90	[100]	$(1.4 \pm 0.1) \times 10^{-16}$
124	250	150	91	0.90	[210]	$(1.8 \pm 0.1) \times 10^{-16}$
723	300	150	90	0.95	[210]	$(7.3 \pm 1.1) \times 10^{-16}$
130	300	150	120	0.87	[210]	$(3.1 \pm 1.2) \times 10^{-16}$
821	300	150	149	0.77	[210]	$(5.1 \pm 0.9) \times 10^{-16}$
919	350	150	18	0.59	[100]	$(3.2 \pm 0.5) \times 10^{-15}$
114	350	150	18	0.59	[210]	$(3.8 \pm 1.3) \times 10^{-15}$
114	350	150	18	0.59	[210]	$(1.4 \pm 0.6) \times 10^{-15}$
713	350	150	18	0.55	[100]	$(1.3 \pm 0.6) \times 10^{-15}$
718	350	150	48	0.94	[210]	$(1.4 \pm 0.2) \times 10^{-15}$
907	450	150	5	0.32	[210]	$(4.0 \pm 2.4) \times 10^{-15}$
716	450	150	22	1.00	[100]	$(5.5 \pm 1.6) \times 10^{-15}$
716	450	150	22	1.00	[210]	$(4.9 \pm 0.9) \times 10^{-15}$
813	450	150	22	0.89	[100]	$(5.4 \pm 1.2) \times 10^{-15}$
118	450	150	22	0.95	[100]	$(7.0 \pm 0.5) \times 10^{-15}$

^{a} D_2O/H_2O ratio (see text)

the first time that micro Raman spectroscopy has been used to determine deuterium diffusion profiles. The advantages of micro Raman spectroscopy over micro IR spectroscopy include better spatial resolution (as small as 1 μm) and simple sample preparation.

The portlandite was analyzed using a Raman microspectrometer (Seki Technotron Co.) after the diffusion experiments. A single monochromator (250IS, Choromex Co.) equipped with a cooled $128 \times 1{,}024$ CCD detector and a 1,200-grooves/mm diffraction grating were used in this study. This diffraction grating enabled us to obtain a Raman spectrum from 1,800–3,900 cm^{-1} in a single measurement. The frequency of the Raman spectra was calibrated using neon emission lines and the intensity of Raman spectra was calibrated using a radiometric calibration standard (LS-1-CAL, Ocean Optics Inc.). The 488-nm line of an Ar^+ laser was used to excite Raman scattering. The laser beam was focused on the sample surface by a microscope objective lens (M Plan Apo SL, Mitutoyo Inc.; magnification: 50, NA: 0.42) giving a beam spot size of ~ 2 μm. The backscattered light was collected using the same lens. The measurement time was varied in the range 30–60 s to obtain spectra having sufficiently high signal-to-noise ratios.

Portlandite has a cleavage parallel to the (001) plane. The crystals were cut by cleaving thin (001) sections of about 20–30 μm from the core of the crystals (Fig. 2a). Thin sections parallel to the (100) plane were also made to obtain diffusion profiles along the c-axis by polishing the crystals embedded in epoxy. Line profiles from the Raman

spectra were measured from the edge of the thin sections to the other edge along the [210] or [100] direction at intervals of 4 μm. Figure 2b shows a line profile along the [210] direction indicated by an arrow in Fig. 2a. In addition, line profile along the [001] direction was determined to investigate deuterium distribution along the c-axis. To accurately determine the Raman band intensities, curve-fitting analysis was performed using GRAMS/AI software (Thermo Galactic Inc.). The Raman bands due to the OD and OH stretching modes in each spectrum were fitted using Lorentzian functions with linear background correction.
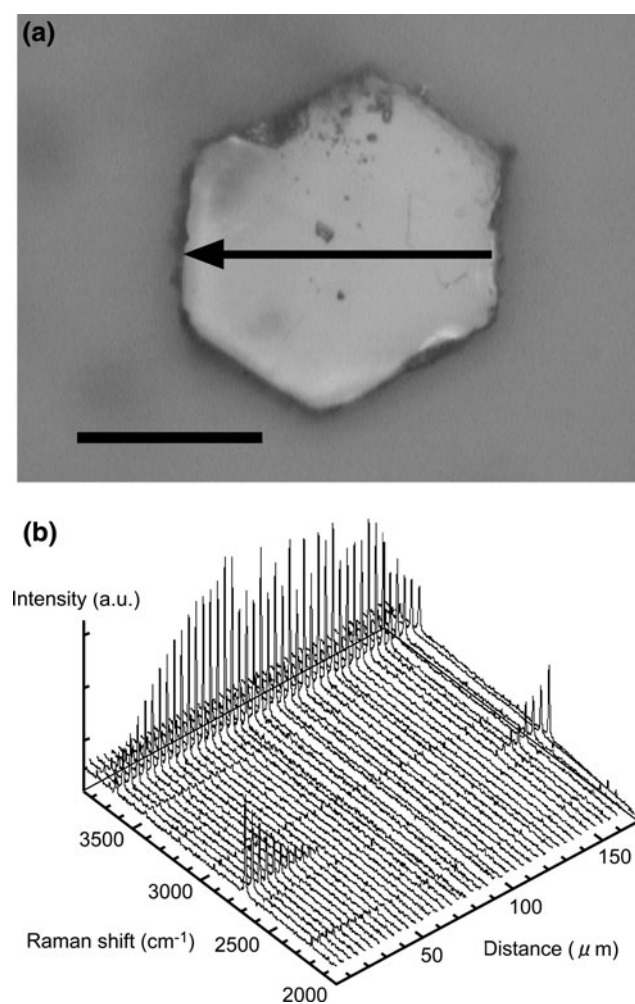

Fig. 2 (a) Photograph of a (001) thin section cut from the crystal after hydrothermal treatment at 300°C and 150 MPa for 90 h (Run. 723; Table 1). The *arrow* in the photograph indicates the [210] direction and the line along which the Raman spectra were obtained. The *scale bar* is 100 μm. (b) Sequential spectra measured at intervals of 4 μm along an *arrow* shown in (a) by a micro Raman spectrometer. Peaks at 2,667 and 3,640 cm^{-1} were assigned to OD and OH stretching vibrations, respectively

Quantitative analysis of deuterium in portlandite using Raman microspectroscopy

In the Raman spectra of partially deuterated portlandite, the relative intensity of the OD stretching mode (A_{1g} normal vibration; 2,667 cm^{-1}) to the OH stretching mode (3,640 cm^{-1}), $I_{OD}/(I_{OD} + I_{OH})$, where I_{OD} and I_{OH} are the intensities of the OD and OH stretching modes respectively, is dependent on the molar ratio of deuterium to hydrogen. The relative intensity of the OD stretching mode to the OH stretching mode varies nonlinearly with the D concentration (Noguchi et al. 2009); therefore, the calibration curve, which represents the relationships between the relative intensity of the OD stretching mode and the molar ratio of deuterium to hydrogen, was determined as follows.

Ca(OD)$_2$ was synthesized by reacting lime (CaO, Wako Co.) powder with deuterated water (D$_2$O). The hydration reaction of lime is highly exothermic and the heat of reaction promotes exchange of D$_2$O in the reactor with H$_2$O vapor in air, thereby preventing pure Ca(OD)$_2$ being synthesized in air. A Y-shaped glass ampoule was used as the reactor to avoid contamination by isotopic exchange. The lime powders were placed in one end of the Y ampoule and heavy water was injected into the other end. The two reagents were mixed after sealing the Y glass ampoule and the sealed ampoule was heated at 180°C for 48 h. The recovered product was confirmed to be Ca(OD)$_2$ by powder X-ray diffraction and IR absorption spectroscopy. The Ca(OD)$_2$ and Ca(OH)$_2$ powders of the reagent were well mixed after determining the mixture ratio by careful weighing. The mixed powders were shaped into pellets. To obtain averaged spectra of the pellets, a rotating sample cell was used that rotates the pellet horizontally during Raman measurements (Noguchi et al. 2009). Each pellet was measured five times with different rotational tracks to reduce error in the data due to the inhomogeneity of the pellets. The deviation of the $I_{OD}/(I_{OD} + I_{OH})$ values of the five spectra was very small: the relative standard deviations for each pellet were less than 2%. Figure 3 shows the relationship between the molar ratio of deuterium to hydrogen, c_{OD}, of the pellets and the relative intensities of the OD bands, $I_{OD}/(I_{OD} + I_{OH})$. By fitting the five data points with the formula proposed by Noguchi et al. (2009), the c_{OD} can be calculated from

$$c_{OD} = \frac{I_{OD}}{I_{OD} + 0.76 I_{OH}}. \tag{6}$$

Optical absorption measurements

Optical absorption measurements of portlandite were conducted using VIS, NIR, and FT-IR microspectrometers under ambient conditions. Mid-IR absorption
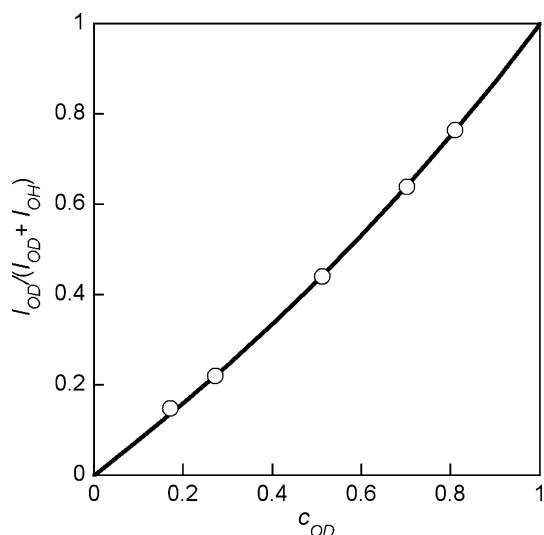
Fig. 3 Correlation between c_{OD} and $I_{OD}/(I_{OD} + I_{OH})$ for Ca(OD)$_2$/Ca(OH)$_2$ mixtures. The *solid line* shows the calibration curve for converting I_{OD} and I_{OH} into c_{OD} (Eq. 6)

spectra (800–4,000 cm^{-1}) were recorded on an FT-IR microspectrometer (FTIR 4200 IMS-1, Shimadzu Co.) equipped with HgCdTe detector. The spectral resolution was 4 cm^{-1}. NIR (4,000–11,000 cm^{-1}) and VIS (11,000–30,000 cm^{-1}) spectra were measured using a lock-in amplifier NIR-VIS microspectrometer (Shinoda et al. 2000). The spectrometer was a single monochrometer (M-10; JASCO Co.) equipped with a PbS detector and a photomultiplier. The resolutions in the NIR and VIS regions were approximately 9 and 5 cm^{-1}, respectively. The frequency of the spectra was calibrated by fitting the positions of the absorption bands of polystyrene with a cubic polynomial. Pellets of powdered portlandite were used as analytical samples. The absorption of the overtone modes was much weaker than that of the fundamental mode, so several pellets were stacked to measure high-order overtone modes. The fundamental, the second, third, and fourth overtone modes of portlandite are shown in Fig. 4a–d, respectively.

Results and discussion

Determination of diffusion coefficient and activation energy

If the migration of deuterium/hydrogen is driven by the concentration gradient, the deuterium/hydrogen flux in the portlandite will obey Fick's first law. Thus, the c_{OD} can be described by a one-dimensional diffusion equation:

$$\frac{\partial c_{OD}(x,t)}{\partial t} = D\frac{\partial^2 c_{OD}(x,t)}{\partial x^2}, \tag{7}$$

where D is the diffusion coefficient, t is the time, and x is the distance. In the case of diffusion in a plane sheet bound by two parallel planes at $x = 0$ and $x = L$, the solution for the diffusion equation can be written as

$$c_{OD}(x,t) = c_0 + \frac{2}{\pi}\sum_{n=1}^{\infty}\frac{c_0\cos n\pi - c_0}{n}\sin\frac{n\pi x}{L}\exp\left(\frac{-Dn^2\pi^2 t}{L^2}\right), \tag{8}$$

where c_0 is the D$_2$O/H$_2$O ratio (Table 1) at the boundaries ($x = 0$ and L) (Crank 1956). The c_{OD} profiles obtained by Raman line analyses are shown in Fig. 5a–d as examples of the analyses. The c_{OD} profile of Fig. 5a was obtained from the Raman profile of Fig. 2b, and the c_{OD} profiles of Fig. 5b–d were obtained from the samples after hydrothermal treatment at 250, 450, 300°C for 145, 22, 120 h, respectively. The diffusion coefficients of each run were determined by least-squares fitting the c_{OD} profiles with Eq. 8 (Table 1). The values of c_0 determined using IR measurements for the recovered fluid in the gold capsule are consistent with the value of c_{OD} at the edges of the thin sections. In addition, some of diffusion coefficients were determined not only by Eq. 8 but by applying the two-dimensional diffusion equation for a cylindrical sample to the diffusion profiles. The two-dimensional diffusion equation and its solution can be expressed as a function of the cylinder radius, r, as follows:

$$\frac{\partial c_{OD}(r,t)}{\partial t} = \frac{1}{r}\frac{\partial}{\partial r}\left(rD\frac{\partial c_{OD}(r,t)}{\partial r}\right), \tag{9}$$

$$c_{OD}(r,t) = c_0\left\{1 - \frac{2}{a}\sum_{n=1}^{\infty}\frac{1}{\alpha_n}\frac{J_0(r\alpha_n)}{J_1(a\alpha_n)}\exp(-D\alpha_n^2 t)\right\}, \tag{10}$$

where a is the radius of the cylindrical sample (=$L/2$), J_n is a Bessel function of order n, and α_n is the root of $(J_n r\alpha_n) = 0$ (Crank 1956). In this study, all diffusion profiles were obtained in the early stages of diffusion, for which the run times for each experiment satisfied $4Dt/L^2$ (or $Dt/a^2) < 0.06$. At such an early stage of diffusion, the diffusion profiles based on one-dimensional and two-dimensional diffusion equations are almost the same as each other. For example, the D values along the [210] direction for Run.723 (Table 1) derived from the one and two-dimensional analyses are 7.3×10^{-16} m^2/s (Fig. 5a) and 6.6×10^{-16} m^2/s, respectively. In this study, we adopted diffusion coefficients from the one-dimensional analyses because of the simplicity of the calculation by the least-squares fitting (Table 1). Furthermore, the c_{OD} profile along the c-axis was determined by Raman analysis through the center of the thin section parallel to the (100) plane. The diffusion profile from the base surface of the crystal to the core is shown in Fig. 5d. It indicates that there is no deuterium at the core of the crystal, namely, the

Fig. 4 (**a**) MIR, (**b, c**) NIR, and (**d**) VIS absorption spectra of portlandite under ambient conditions. Absorption bands due to the (**a**) fundamental mode and (**b**) 2nd, (**c**) 3rd, and (**d**) 4th overtone modes of OH stretching vibration
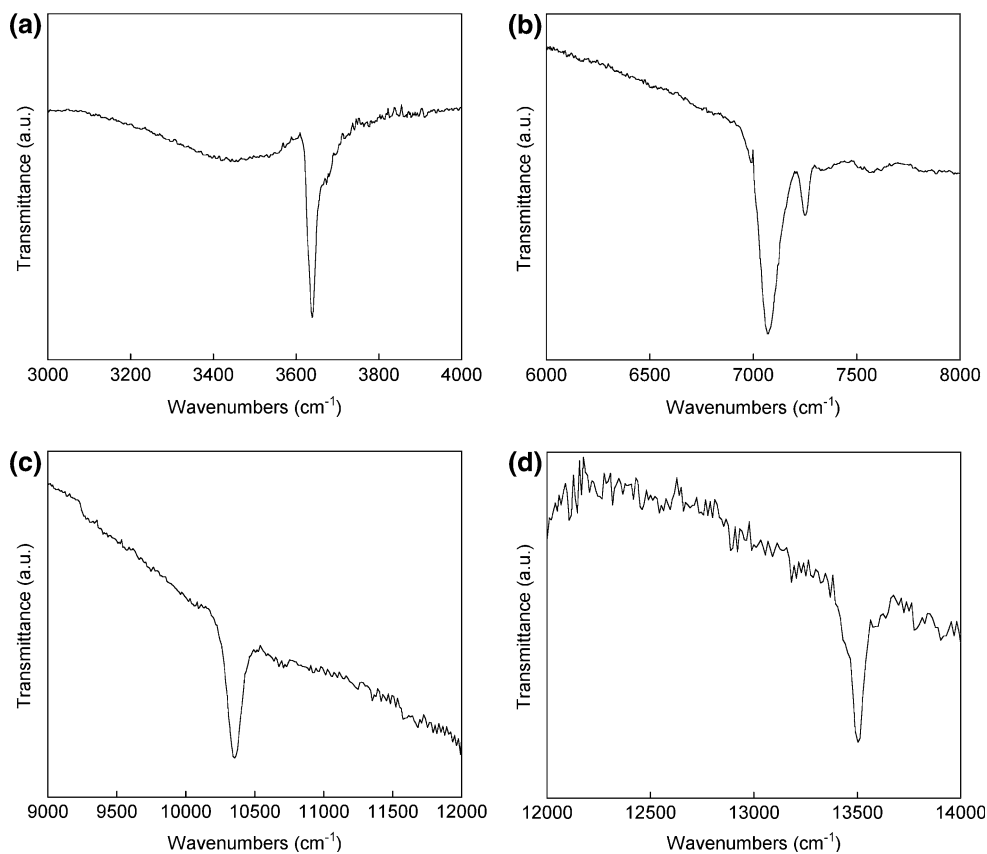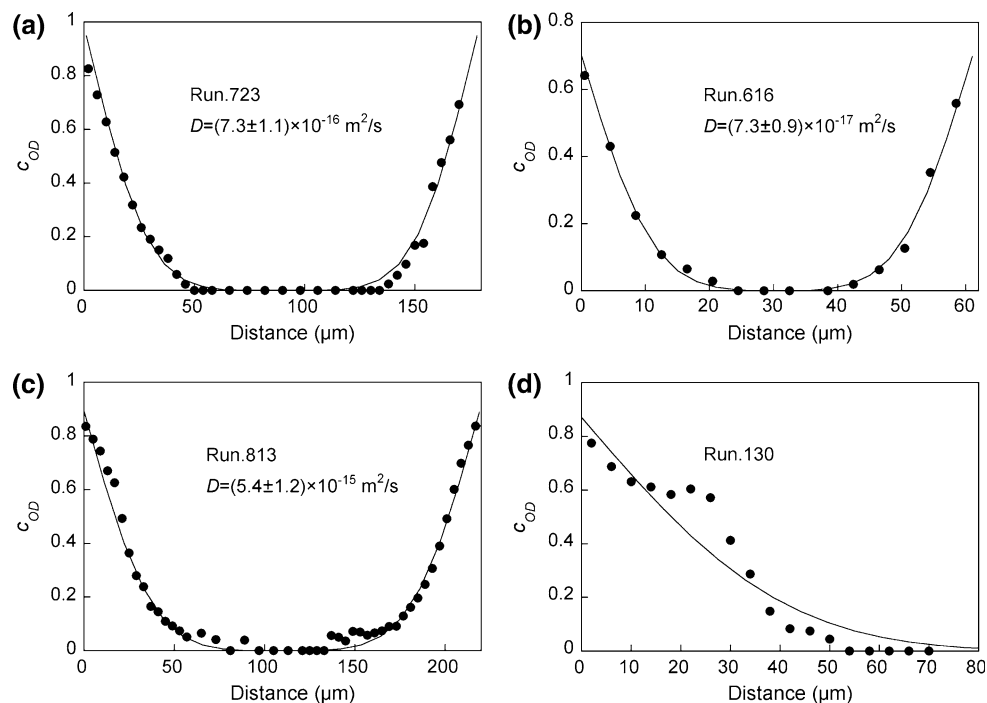

Fig. 5 (**a–c**) The profiles of the molar ratio of deuterium to hydrogen (c_{OD} profile) perpendicular to the *c*-axis for various experimental conditions. The *solid lines* indicate the least-squares fit of Eq. 8 to the data. (**d**) The c_{OD} profile along the *c*-axis. The base surface of the crystal was 0 μm, and the central position is 80 μm from the base surface

deuterium diffused from the base surface along the *c*-axis had not reached the core. The thin sections parallel to the (001) plane were cut from core of the crystal; therefore, the *D* values perpendicular to the *c*-axis determined from

experimental data were not affected by deuterium atoms that diffused along the *c*-axis.

No significant difference was noted between the *D* values determined along the [100] and [210] directions

(Table 1). Arrhenius parameters, activation energy (E) and frequency factor (pre-exponential factor, D_0) perpendicular to the c-axis are determined from the slope and intercept of Arrhenius plot of the diffusion coefficients (Fig. 6), respectively. The Arrhenius equation is

$$D = 1.0 \times 10^{-10} \exp\left[-\frac{0.61 \pm 0.03 \text{ eV}}{kT}\right] (\text{m}^2/\text{s}), \qquad (11)$$

where k is the Boltzmann constant. The diffusion perpendicular to the c-axis of portlandite is fast compared to proton diffusion in other hydrous minerals. Proton diffusion in a crystal must be strongly related to the crystal structure. In this case, there are no atoms that disturb protons jumping between the proton sites. The faster proton diffusion in portlandite is thought to be caused by the shorter distances between the proton sites compared with other hydrous minerals.

Proton diffusion mechanism

Microscopic mechanisms of self-diffusion of atoms in crystals can typically be categorized into two types: the vacancy mechanism and the interstitial mechanism (Borg and Dienes 1988). In the vacancy mechanism, the diffusion jump occurs by a proton exchanging positions with a neighboring vacancy. By contrast, in the interstitial mechanism, a diffusing atom migrates via sites located between rational lattice sites. The vacancy mechanism is
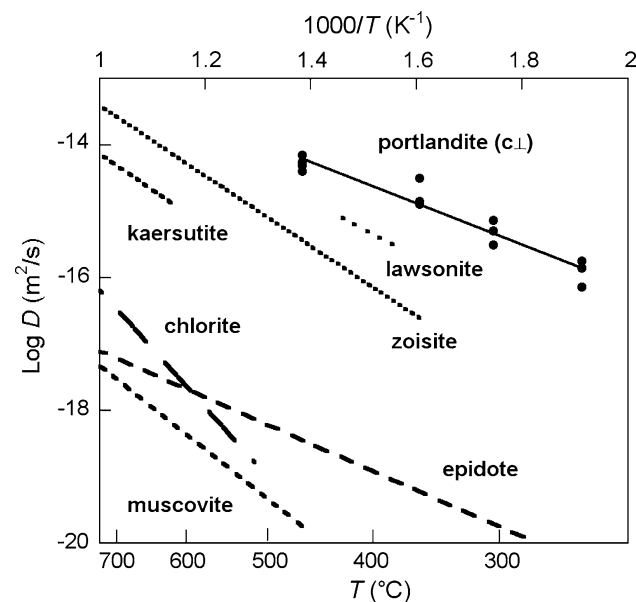

Fig. 6 Arrhenius plots of D perpendicular to the c-axis of portlandite and D of various hydrous minerals. The *solid line* is the least-squares fit to the portlandite data. Data for lowsonite, kaersutite, muscovite, and chlorite are from Marion et al. (2001), Ingrin and Blanchard (2000) and Graham et al. (1987), respectively, and those for epidote and zoisite are from Graham (1981)

thought to be the dominant mechanism of proton diffusion perpendicular to the c-axis of portlandite, because there are no possible interstitial sites in the proton layer. The space between two neighboring protons in the proton layer is unstable as the interstitial site of proton because of the proton-proton repulsive interaction. The interstitial mechanism, however, plays an important role in proton diffusion parallel to the c-axis. Protons diffuse via interstitial sites in the $[\text{CaO}_6]$ layer, which are quasi-stable and are not detectable by X-ray and neutron diffraction techniques.

For one of the three protons neighboring a vacant site to jump to the vacant site, the proton must overcome the potential energy barrier between the two oxygen atoms. In general, a vacancy can be formed by either intrinsic or extrinsic mechanisms (Borg and Dienes 1988). In the intrinsic mechanism, vacancies are thermally generated at relatively high temperatures. When vacancies generated by the intrinsic mechanism control proton diffusion, the diffusion activation energy is equal to the sum of the formation energy of thermally generated vacancies and the proton migration energy. On the other hand, in the extrinsic mechanism, vacancies are introduced to compensate the charge balance due to impurities in the structure. The activation energy of the extrinsic mechanism is simply the activation energy of proton migration. The extrinsic vacancy mechanism must control the proton diffusion observed in this investigation, because differential thermal analysis by Bai et al. (1994) indicated that intrinsic vacancies of protons were not formed in portlandite by dehydration up to 450°C. Furthermore, Matsunaga and Kuwabara (2007) suggested that an energy as high as about 1.5 eV is required to introduce a proton vacancy into a covalent OH bond. The self-diffusion activation energy (E) of portlandite was 0.61 eV, which is too low to be explained by the intrinsic mechanism. Therefore, this value is attributed to the activation energy when a proton migrates to a neighboring vacant site.

Estimation of potential barrier height

When a proton migrates to a neighboring vacant site, we assume that the proton does not jump directly from a $6i$ site to the vacant site, but undergoes the following processes. We estimate the potential barrier height based on the migration model. A proton generally hops between the three $6i$ sites because of the almost flat potential barriers between the three $6i$ sites (Fig. 7). In addition to this hopping motion, the OH dipole can easily tilt away from the $6i$ site due to the very low tilting energy and this causes the proton to move to the H_1' site (see Fig. 7). According to Matsushita (2001), the tilting motion requires only 0.01 eV. When the proton moves to the H_1' site and the equivalent H_2' site is vacant, the jumping path is minimized
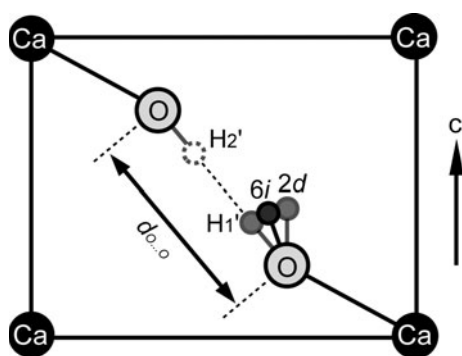
Fig. 7 The (110) section of the unit cell including a proton vacancy. $2d$ and $6i$ are Wyckoff sites. H_1' and H_2' are positions occupied by a proton on tilting of the OH dipole so that H_1' and H_2' and two oxygen atoms become aligned. The jump path is minimized when a proton moves to the H_1' position, and the proton jumps to the vacant H_2' position via the H_1' position. $d_{O\cdots O}$ indicates the interlayer oxygen distance

allowing the proton to jump to the neighboring site with the lowest expenditure of energy. In such a proton migration process, the activation energy for a proton to migrate from a $6i$ site to its neighboring site is mainly the energy to overcome the potential barrier between H_1' and H_2'. The potential energy curve between H_1' and H_2' can be deduced from overlapping OH_1'-PEC and OH_2'-PEC at an interval of the interlayer oxygen distance ($d_{O\cdots O}$, in Fig. 7), and the potential barrier may be estimated. The intersection of the OH_1'-PEC and the OH_2'-PEC is a saddle point in the potential energy curve between the two oxygen atoms, and the energy of the saddle point corresponds to the potential barrier (Eyring 1941). In the following, we assume that an OH-PEC determined by the optical absorption measurements corresponds to OH_1'-PEC and OH_2'-PEC, and we estimate the potential barrier by overlapping the two OH-PECs.

An OH-PEC can be determined from the wavenumbers of the OH absorption bands. By substituting the four wavenumbers from the fundamental mode (ω_1) to the fourth overtone mode (ω_4) in Table 2 into Eq. 5, four simultaneous equations for ω_e and χ are formed. And the

Table 2 List of frequencies of fundamental and overtone modes for OH stretching vibration and their pressure dependency

n	$\omega_n - \omega_0$ (cm^{-1})	$G(n) - G(0)$ (eV)
0	0	0
1	3,645	0.45
2	7,067	0.88
3	10,341	1.28
4	13,501	1.67

ω_0 is 1,870 cm^{-1}, which was estimated from $G(0)$

most probable ω_e and χ were, respectively, determined to be 3781 ± 29 cm^{-1} and 0.0216 ± 0.0057 by the method of least squares for the simultaneous equations. The D_e and α in the Morse potential equation (Eq. 1) were derived from Eqs. 3 and 4. The estimated OH-PEC is:

$$U(r) = (5.54 \pm 1.43)\,(1 - \exp[-(2.11 \pm 0.63)$$
$$\times (r - r_0)])^2 (eV). \tag{12}$$

The OH-PEC described by Eq. 12 is shown in Fig. 8a. To estimate the potential energy barrier, the two OH-PECs are simply overlapped here at the interval of the equilibrium $d_{O\cdots O}$, which is 3.32 Å at room temperature and 0.5 GPa (Nagai et al. 2000). Figure 8b shows the two overlapping OH-PECs, and it indicates that the energy at the intersection point of the two OH-PECs is 3.35 eV. Subtracting the zero-point energy of the proton ($G(0)$), it was determined to be 0.24 eV from Eq. 2, from the value of the intersection gives the energy of the potential barrier (3.11 eV) that a proton needs to overcome to jump to neighboring proton sites. The E determined by the diffusion experiments is 0.61 eV. Therefore, the potential barrier for the equilibrium distance of 3.32 Å is too high to be the activation energy of proton diffusion.

This high potential energy barrier must be due to the following two factors, which have not been considered in the above estimation. The first factor is that the oxygen at the vacancy site has an excess electron due to a dangling bond. The oxygen atom becomes negatively charged by the excess electron, which increases the electrostatic force between the oxygen and the proton. The energies of the OH_1'-PEC and OH_2'-PEC are lowered by the electrostatic interaction as shown in Fig. 9a, and the potential barrier is reduced. The second factor is the thermal vibrations of oxygen atoms. The interlayer oxygen distance, $d_{O\cdots O}$ deviates from the equilibrium distance as a result of such vibrations. When $d_{O\cdots O}$ is shorter than the equilibrium distance, the potential barrier is lowered by shortening of the jumping path (Fig. 9b). These two factors are thought to be responsible for reducing the potential barrier to 0.61 eV.

The jumping frequency of a proton

Analyzing the frequency factor (D_0) is valuable for understanding the microscopic mechanism of diffusion, because it is related to the jumping rate for diffusing atoms. When an atom bonded in a crystal migrates to the nearest neighboring site by jumping, Fick's first law for the atom flux, J, can be expressed as

$$J = -l^2 v \frac{\partial c}{\partial x}, \tag{13}$$

where l is the jump distance, which is equivalent to the distance to the neighboring site, and v is the jump
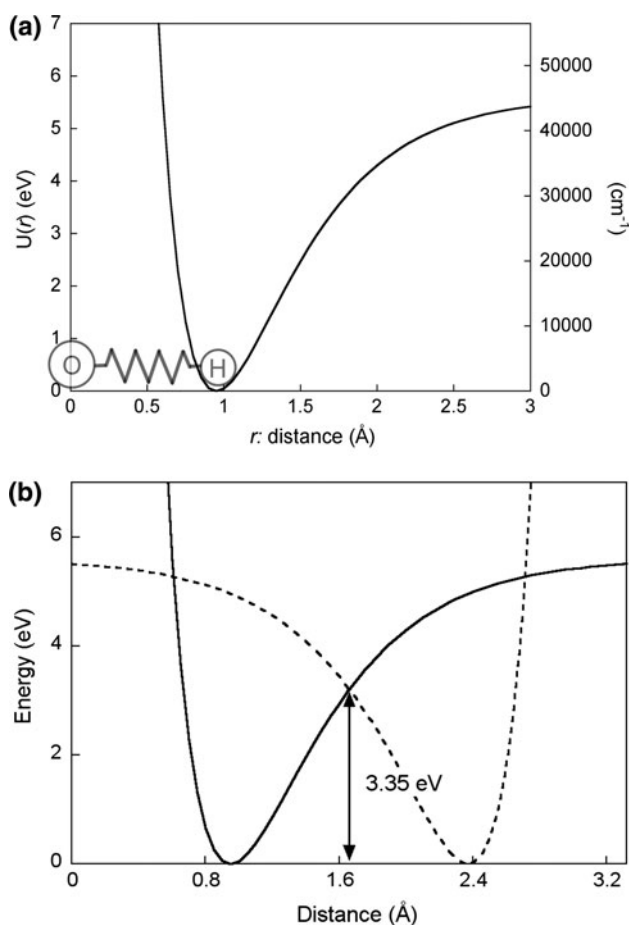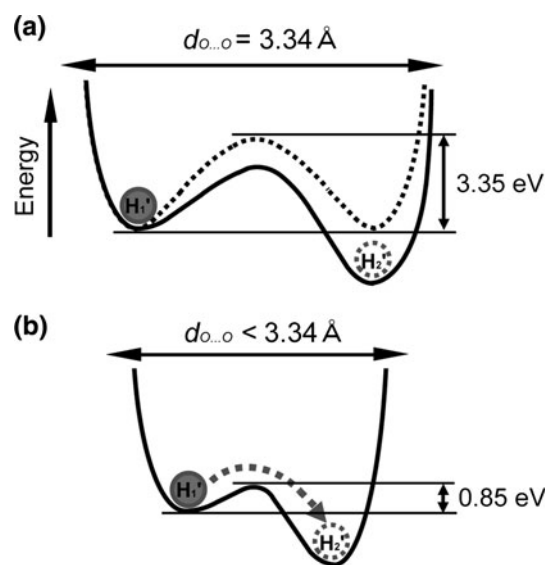
Fig. 9 a Schematic image to lower the potential barrier by the electrostatic interaction between the negatively charged oxygen and the proton. The *broken line* is the potential energy barrier determined by simply overlapping two OH-PECs determined from the present spectroscopic measurements (Fig. 8b). **b** Schematic image of the potential barrier at the instant when the potential barrier height reduced to 0.61 eV by the shrinking $d_{O\cdots O}$. The "0.85 eV" in the figure is the sum of the zero point energy of proton, $G(0) = 0.24$ eV and the potential barrier height, 0.61 eV

Fig. 8 a The potential energy curve of OH (OH-PEC) of portlandite determined from spectroscopic measurements. **b** A potential barrier between two oxygen atoms across the proton layer of portlandite. The *solid line* and *broken line* indicate OH_1'-PEC and OH_2'-PEC which are given by Eq. 12, respectively. The H_1' position is occupied by the proton and the H_2' position is vacant (see Fig. 7). They are overlapped at an interval of 3.32 Å

frequency (Borg and Dienes 1988). In the case of the vacancy mechanism, D_0 can be related to l and v in Fick's first law as follows:

$$D_0 = \frac{1}{2d} f\, l^2\, X_v\, v. \tag{14}$$

In the above equation, d is the dimension of the diffusible medium. In the case of diffusion in the proton layer of portlandite $d = 2$. f is the tracer correlation factor, which relates to the crystal structure. f is determined to be 1/2 by considering the geometry of the crystal structure (honeycomb lattice) (Borg and Dienes 1988). For diffusion perpendicular to the c-axis, l is the distance between two proton sites across a proton layer. Here the splitting of proton sites by disorder is neglected and the distance between two $2d$ sites (2.18 Å, Xu et al. 2007) is substituted for l in Eq. 14. X_v is the fraction of vacant sites and for the

extrinsic vacancy mechanism it corresponds to the impurity concentration in the crystal, as mentioned above. Based on the purity of the reagent Ca(OH)$_2$ (99.9%), X_v must be of the order of 1.0×10^{-3}. Substituting the above values into Eq. 14, gives a jump frequency, v, of 1.7×10^{13} Hz. This jump frequency is of the same order as the frequencies of the lattice vibration modes of [CaO$_6$] ($\sim 10^{13}$ Hz). This indicates that the reduction in $d_{O\cdots O}$ induced by thermal vibrations may control proton jumping.

For proton diffusion at a pressure as high as 150 MPa, the effects of splitting of proton sites and dynamic disorder were not remarkable. However, they must affect the proton diffusion mechanism at high pressure and high temperature. The large splitting between the three disorder sites and dynamic hopping between their sites must control proton diffusion. Such a novel diffusion mechanism, which does not depend on the thermal vibrations of oxygen atoms, may be induced by pressure. It is important to investigate this experimentally and by computer simulations.

References

Bai TB, Koster van Groos AF, Guggenheim S (1994) Phase transition, dehydration, and melting relationships of portlandite. Am Min 79:1223–1226

Boettcher AL, Kerrick DM (1971) Temperature calibration in cold-seal pressure vessels. In: Ulmer GC (ed) Research techniques for high pressure and high temperature. Springer, New York

Borg RJ, Dienes GJ (1988) An introduction to solid state diffusion. Academic Press, London

Crank J (1956) Mathematics of diffusion. Oxford University Press, New York

Desgranges L, Grebille D, Calvarin G, Chevrier G, Floquet N, Niepce JC (1993) Hydrogen thermal motion in calcium hydroxide. Acta Cryst B49:812–817

Eyring H (1941) The theory of rate processes. McGraw-Hill, New York

Graham CM (1981) Experimental hydrogen isotope studies III: diffusion of hydrogen in hydrous minerals, and stable isotope exchange in metamorphic rocks. Contrib Miner Petrol 76:216–228

Graham CM, Viglino JA, Harmon RS (1987) Experimental study of hydrogen-isotope exchange between aluminous chlorite and water and hydrogen diffusion in chlorite. Am Miner 72:566–579

Herzberg G (1989) Molecular spectra and molecular structure, vol 1, 2nd edn. Krieger, Florida

Ingrin J, Blanchard M (2000) Hydrogen mobility in single crystal kaersutite. EMPG VIII, J Confe Abstr 5:52

Ingrin J, Blanchard M (2006) Diffusion of hydrogen in minerals. In: Keppler H, Smyth JR (eds) Water in nominally anhydrous minerals. Rev Miner Geochem 62:291–320

Ingrin J, Skogby H (2000) Hydrogen in nominally anhydrous upper-mantle minerals: concentration levels and implications. Eur J Miner 12:543–570

Kurka A, Blanchard M, Ingrin J (2005) Kinetics of hydrogen extraction and deuteration in grossular. Miner Mag 69:359–371

Marion S, Meyer HW, Carpenter M, Norby T (2001) H_2O–D_2O exchange in lawsonite. Am Miner 86:1166–1169

Matsunaga K, Kuwabara A (2007) First-principles study of vacancy formation in hydroxyapatite. Phys Rev B 75:014102

Matsushita E (2001) Tunneling mechanism on proton conduction in perovskite oxides. Solid State Ionics 145:445–450

Morse PM (1929) Diatomic molecules according to the wave mechanics. II: vibrational levels. Phys Rev 34:57–64

Nagai T, Ito T, Hattori T, Yamanaka T (2000) Compression mechanism and amorphization of portlandite, $Ca(OH)_2$: structural refinement under pressure. Phys Chem Miner 27:462–466

Noguchi N, Shinoda K, Masuda K (2009) Quantitative analysis of binary mineral mixtures using Raman microspectroscopy: calibration curves for silica and calcium carbonate minerals and application to an opaline silica nodule of volcanic origin. J Miner Petrol Sci 104:253–262

Parise JB (2006) High pressure studies. In: Wenk HR (ed) Neutron scattering in earth sciences. Rev Miner Geochem 63:205–231

Raugei S, Silvestrelli PL, Parrinello M (1999) Pressure-induced frustration and disorder in $Mg(OH)_2$ and $Ca(OH)_2$. Phys Rev Lett 83:2222–2225

Shinoda K, Nagai T, Aikawa N (2000) Pressure-dependent anharmonic coefficient of OH in portlandite by NIR-IR spectroscopy with DAC. J Miner Petrol Sci 95:65–70

Venyaminov SY, Prendergast FG (1997) Water (H_2O and D_2O) molar absorptivity in the 1,000–4,000 cm^{-1} range and quantitative infrared spectroscopy of aqueous solutions. Anal Biochem 248:234–245

Xu H, Zhao Y, Zhang J, Hickmott DD, Daemen LL (2007) In situ neutron diffraction study of deuterated portlandite $Ca(OD)_2$ at high pressure and temperature. Phys Chem Miner 34:223–232